JOURNAL OF APPLIED ELECTROCHEMISTRY **26** (1996) 795–802

Current distribution in aluminium electrolysis cells with Søderberg anodes
Part II: Mathematical modelling

J. ZORIC, I. ROUSAR, Z. KUANG

University of Chemical Technology, Department of Inorganic Technology, 16628 Prague 6, Czech Republic

J. THONSTAD

Department of Electrochemistry, Norwegian Institute of Technology, N-7034, Trondheim, Norway

Received 14 August 1995; revised 11 December 1995

The current distribution in an aluminium electrolysis cell with a Søderberg anode was calculated to supplement measured data (Part I of this study). A numerical method based on the conservative scheme was used. A 2D cross section of a commercial cell was considered and the electric fields in the anode, cathode and the electrolyte were considered under steady state conditions. Four different approximations of a curvilinear boundary were proposed. The overvoltage for both electrodes was introduced. The current density decreased along the side of the anode from the nominal value 0.8 A cm^{-2} on the underside to 0.26 A cm^{-2} in the upper part near the surface of the electrolyte. The calculated current density along the side of the Søderberg anode for all the approximations was compared with the measured data, and the agreement was within 10 to 15%. In the curved part of the anode the differences between measured and calculated values were 20–28%; but in this region the accuracy of the experimental data was in the same range. Also the finite element method was used for the comparison of the calculated current density.

List of symbols

d, l, w	height, length and width of the unit cell (cm), see Figs 2 and 4
l_{av}	length of the diagonal line used for averaging, see Fig. 10
E	electrode potential (V)
I	current (A)
$I_{1,2}$, $I_{2,1}$, $I_{3,4}$, $I_{4,3}$	currents flowing in and out the cell (i,j), see Equations 18–22 and Fig. 4
$I_{4,1}$, $I_{2,3}$, $I_{4,2}$, $I_{2,4}$...	diagonal currents, see Fig. 6, and Equations 34–37
j	current density (A cm^{-2})
$R(i,j)$	residuum, see Equations 24 and 25
S	area perpendicular to the current flow (cm^2)
U	cell voltage (V)

Greek symbols

η	overvoltage (V)
φ	Galvani potential (V)
ρ	specific resistivity (Ω cm)

Subscripts

A	anode
A1	in the anode stud, see Fig. 3
avr	averaged value
C	cathode
E	electrolyte
E2	in the bulk of the electrolyte, see Fig. 3
loc	local values
rev	reversible

Superscripts

E	in the electrolyte at the interface, see Fig. 1
S	in the metallic phase at the interface, see Fig. 1
M	in the metallic phase, see Fig. 1

1. Introduction

Part I of this paper [1] treated an experimental study of the current distribution along the side of the anode in aluminium electrolysis cells of the Søderberg type. A voltage probe attached to a position sensor was used to map the potential distribution in the side channel of the cells, and the current distribution along

0021-891X

the side of the anode was derived from this data. Due to some scatter in the measured data, and problems in positioning the probe under the curved part of the anode, it was decided to check the experimental data against a 2D mathematical model. The purpose of this second paper is to identify the electrical field distribution in Søderberg aluminium cells [2, 3], considering the electric field in the anode, electrolyte and cathode, and taking into account the effects of the anodic and cathodic overvoltages. The conservative scheme for the solution of the Laplace equation in 2D space [4, 5] was used. Steady state conditions were assumed, and any influence on the electric field by the temperature or by the magnetic field was not considered.

2. Mathematical description of the 2D model

An electrolytic cell consisting of anode, cathode and electrolyte was considered taking the anode as the most positive part of the system, and the cathode as the most negative. The cell voltage, U, was therefore given as the difference between the Galvani potential in the anode busbar φ_A^M, and in the cathodic busbar φ_C^M,

$$U = \varphi_A^M - \varphi_C^M \tag{1}$$

The shape of the anode and of the wall of the cavity, which is limited by a ledge of frozen electrolyte, was measured in Part I of this work [1]. A typical shape is shown in Fig. 1. The difference of Galvani potentials in Equation 1 can simply be changed into the difference between voltage drops along any current line going from the anode to the cathode.

$$U = (\varphi_A^M - \varphi_A^S) + (\varphi_A^S - \varphi_A^E) + (\varphi_A^E - \varphi_C^E) + (\varphi_C^E - \varphi_C^S) + (\varphi_C^S - \varphi_C^M) \tag{2}$$

The Galvani potentials of the anode and the cathode represent the cell voltage. From Equation 2 it follows that the cell voltage consists of

$\varphi_A^M - \varphi_A^S$, the voltage drop (ohmic) in the anode material

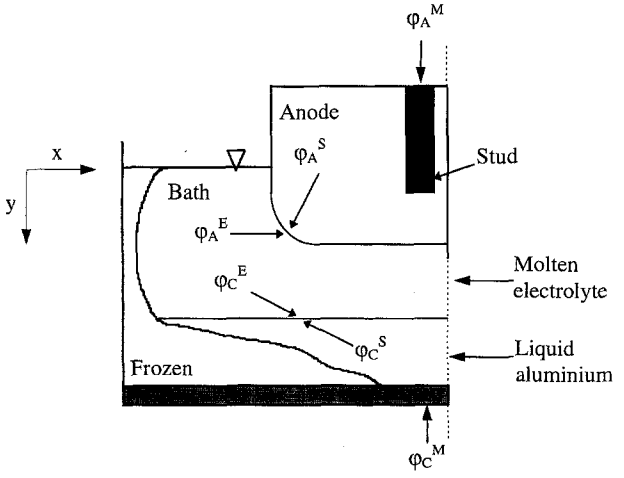

Fig. 1. Sketch of a cross section of a part of an aluminium cell with a Søderberg anode.

$\varphi_A^S - \varphi_A^E$, the potential of the anode (E_A)
$\varphi_A^E - \varphi_C^E$, the voltage drop in the electrolyte
$\varphi_C^E - \varphi_C^S$, the potential of the cathode ($-E_C$)
$\varphi_C^S - \varphi_C^M$, the voltage drop in the cathode material.

The definition of the anode potential is given by Equation 3:

$$E_A = \varphi_A^S - \varphi_A^E + \text{constant} \tag{3}$$

where the constant depends on the reference electrode used. The constant may be set equal to zero without any loss of information. The same is valid for the cathode:

$$E_C = \varphi_C^S - \varphi_C^E + \text{constant} \tag{4}$$

The electrode potentials are the sum of the reversible potential and an overvoltage:

$$E_A = E_{rev,A} + \eta_A(j_{n,A}) \tag{5}$$

$$E_C = E_{rev,C} + \eta_C(j_{n,C}) \tag{6}$$

The reversible cell voltage $E_{rev,cell}$ is given by Equation 7:

$$E_{rev,cell} = E_{rev,A} - E_{rev,C} \tag{7}$$

with the assumption $E_{rev,C} = 0$

Using Equations 3–7 we can rewrite Equation 1 or 2 in the following way:

$$U = E_{rev,cell} + \eta_A(j_{n,A}) - \eta_C(j_{n,C}) + (\varphi_A^M - \varphi_A^S) + (\varphi_A^E - \varphi_C^E) + (\varphi_C^S - \varphi_C^M) \tag{8}$$

The last three terms in Equation 8 represent ohmic losses in the anode material, the electrolyte and in the cathode material. To calculate these values, Ohm's law in vector notation was introduced:

$$\boldsymbol{j} = -\frac{1}{\rho}\nabla\varphi \tag{9}$$

For the unidirectional case (in the direction of the x coordinate; for the definition of the coordinate system, see Fig. 4);

$$j_x = -\frac{1}{\rho}\frac{\partial\varphi}{\partial x} \tag{10}$$

If we assume that the specific resistivity is constant along a current line of length l, integration of Equation 10 leads to

$$\varphi_1 - \varphi_2 = j\rho l \tag{11}$$

In many cases it is more useful to use the current I, instead of the current density j,

$$j = I/S \tag{12}$$

The voltage drop in an element as shown in Fig. 2 is

$$\varphi_1 - \varphi_2 = I\rho(l/S) \tag{13}$$

where the potentials φ_1 and φ_2 are the potentials at the sides of the unit cell. A space with changing specific resistivity (in 1D, 2D or 3D space) can be treated as a set of elements, each with a constant specific

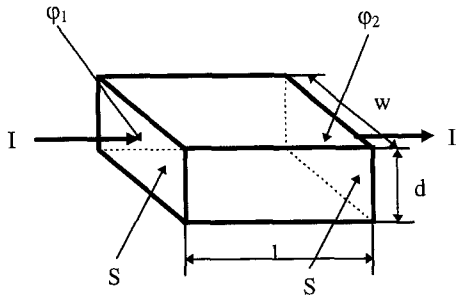

Fig. 2. Spatial element with constant specific resistivity.

resistivity ρ,

$$\varphi_1 - \varphi_2 = I[\rho_1(l_1/S_1) + \rho_2(l_2/S_2)] \quad (14)$$

On the boundary between two neighbouring elements a voltage drop may be present. This voltage drop is the potential E of the anode or cathode, see Fig. 3.

For the anode,

$$\varphi_{A,1} - \varphi_A^S = I\rho_A(l_A/S) \quad (15a)$$

$$\varphi_A^S - \varphi_A^E = E_A \quad (15b)$$

$$\varphi_A^E - \varphi_{E,2} = I\rho_E(l_E/S) \quad (15c)$$

Adding Equations 15(a), 15(b) and 15(c) we obtain

$$(\varphi_{A,1} - \varphi_{E,2} - E_A) = I[\rho_A(l_A/S) + \rho_E(l_E/S)] \quad (16)$$

where $\varphi_{A,1} - \varphi_{E,2} - E_A > 0$ and $I > 0$.

Figure 3 is valid for the so-called rectangular grid. The potentials φ_{A1} and φ_{E2} are the potentials of the points located in the middle of the cells in the neighbourhood of the anode boundary.

In Fig. 4 a rectangular grid in 2D space is shown. The fluxes are denoted with bold letters (**I**), and the boundary indices (m) of the calculation unit in italics. The figure shows the so-called central cell (i,j) surrounded by its neighbouring points.

The currents flowing in and out of the cell (i,j) are denoted $I_{1,2}$, $I_{2,1}$, $I_{3,4}$, $I_{4,3}$. In the following equations $A(i,j,k,l)$ represent the voltage drop on the boundary $k|l$. This voltage drop is equal to the electrode potential on the electrode/electrolyte boundary. In the electrolyte or in the electrode material $A(i,j,k,l)$ is

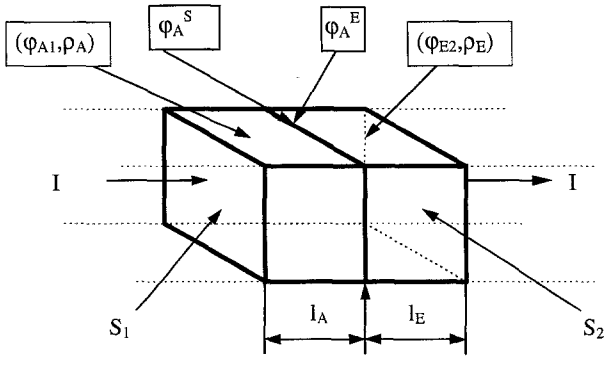

Fig. 3. Two spatial elements with different specific resistivities. The potentials φ_{A1}, and φ_{E2} are the potentials of the points located in the middle of the cells in the neighbourhood of the anode boundary. The potential φ_A^S is located at the anode surface (in the anode material) and the potential φ_A^E is located at the anode surface in the electrolyte.

equal to zero. For example, current going from the boundary line $m = 1$ to the line $m = 2$ of the neighbouring unit is written as

$$\mathbf{I}_{1,2} = -\frac{\varphi(i-1,j) - \varphi(i,j) - A(i,j,1,2)}{\rho(i-1,j)\frac{d}{2d} + \rho(i,j)\frac{d}{2d}} \quad (17)$$

Equation 17 may be rewritten as:

$$\mathbf{I}_{1,2} = -2\frac{\varphi(i-1,j) - \varphi(i,j) - A(i,j,1,2)}{\rho(i-1,j) + \rho(i,j)} \quad (18)$$

where

$A(i,j,1,2) = E_A$ if $\varphi(i-1,j)$ is located in the anode material and $\varphi(i,j)$ is located in the electrolyte,

$A(i,j,1,2) = -E_A$ if $\varphi(i-1,j)$ is located in the electrolyte and $\varphi(i,j)$ is located in the anode material,

$A(i,j,1,2) = 0$ for both potentials located in the anode or cathode material boundary, or in the electrolyte.

Similar relations can be found for the boundaries $m = 2$, 3 and 4.

$$\mathbf{I}_{2,1} = -2\frac{\varphi(i+1,j) - \varphi(i,j) - A(i,j,2,1)}{\rho(i+1,j) + \rho(i,j)} \quad (19)$$

$$\mathbf{I}_{3,4} = -2\frac{\varphi(i,j-1) - \varphi(i,j) - A(i,j,3,4)}{\rho(i,j-1) + \rho(i,j)} \quad (20)$$

$$\mathbf{I}_{4,3} = -2\frac{\varphi(i,j+1) - \varphi(i,j) - A(i,j,4,3)}{\rho(i,j+1) + \rho(i,j)} \quad (21)$$

At steady state the integral of the current density normal to the surface has to be zero:

$$\oint j_n \, dS = 0 \quad (22)$$

Equations 18–21 can be used for the evaluation of Equation 22, if there are only the above mentioned four fluxes:

$$\mathbf{I}_{1,2} + \mathbf{I}_{2,1} + \mathbf{I}_{3,4} + \mathbf{I}_{4,3} = 0 \quad (23)$$

On the basis of Equation 23 the residuum $R(i,j)$ can be introduced in Equation 24,

$$R(i,j) = 2\left[\frac{\varphi(i-1,j) - \varphi(i,j) - A(i,j,1,2)}{\rho(i-1,j) + \rho(i,j)} + \frac{\varphi(i+1,j) - \varphi(i,j) - A(i,j,2,1)}{\rho(i+1,j) + \rho(i,j)} + \frac{\varphi(i,j-1) - \varphi(i,j) - A(i,j,3,4)}{\rho(i,j-1) + \rho(i,j)} + \frac{\varphi(i,j+1) - \varphi(i,j) - A(i,j,4,3)}{\rho(i,j+1) + \rho(i,j)}\right] \quad (24)$$

Equation 23 is satisfied if for all points (i,j) in the 2D space:

$$R(i,j) = 0 \quad (25)$$

Equation 25 represents the so-called conservative

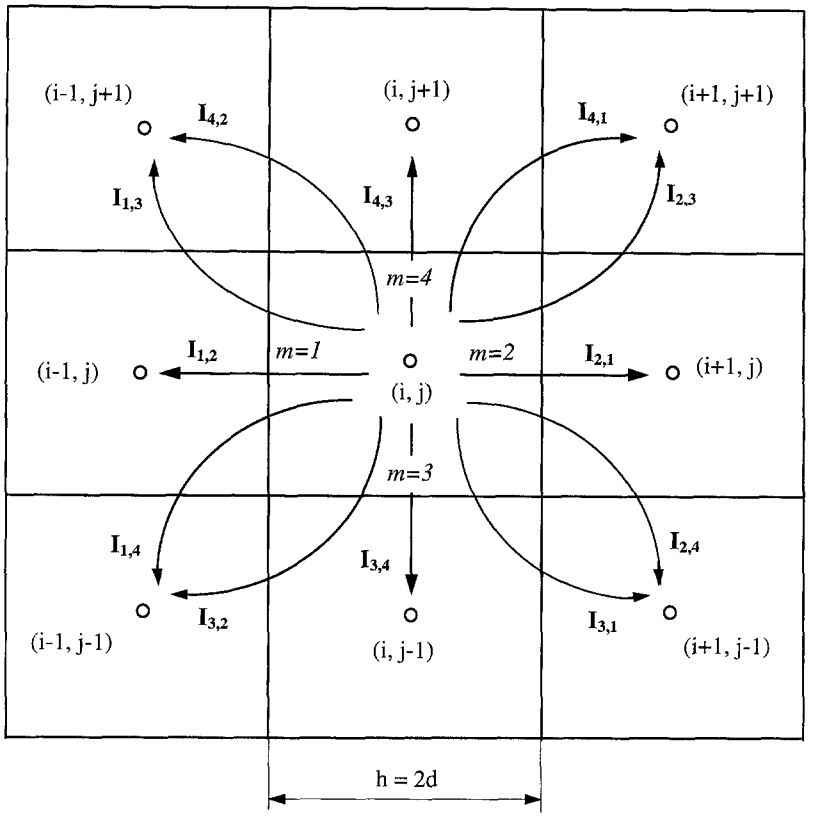

Fig. 4. Notation of currents for a rectangular grid in 2D space. The fluxes are denoted with bold letters (**I**) and the indices follow the notation of boundaries left by the current. Boundary indices (m) of the calculation unit are written in italics.

scheme for the calculation of Galvani potentials in the considered space. 'Conservative' simply means that all the current which flows into the cell also flows out of the cell. The conservative scheme with residuum $R(i,j)$, given by Equation 24, also fulfils the Laplace equation for a space with varying specific resistivity:

$$\nabla\left(\frac{1}{\rho}\nabla\varphi\right) = 0 \tag{26}$$

Equation 26 can also be approximated in such a way that the conservation of current is not preserved. The most well-known nonconservative approach uses the finite difference method.

3. Assumptions

In the case under study the following assumptions were made:

(i) The voltage drop in the cathode metal was neglected.

(ii) The Galvani potential of the cathode was set to zero.

$$\varphi_C^M = 0 \tag{27}$$

(iii) From Equations 27 and 1 it follows that

$$\varphi_A^M = U \tag{28}$$

The Galvani potential of the steel studs in the anode (see Fig. 1) was set equal to the cell voltage.

(iv) Input data for the calculations were taken for a typical industrial cell [1, 2, 3, 6]:

specific resistivity of the Søderberg anode: 0.008 Ω cm [1]

specific resistivity of the electrolyte: 0.465 Ω cm valid for the following composition and temperature: 11 wt % AlF_3, 5 wt % CaF_3, 3 wt % Al_2O_3, 960 °C = 1233 K.

(v) For the cathode overvoltage a linear polarization curve was assumed, with

$$\eta_C = -0.08|j| \tag{29}$$

Using Equations 27, 29 and 4 we obtain

$$\varphi_C^E = -\eta_C \tag{30}$$

It follows that the Galvani potential at the cathode surface from the electrolyte side is equal to the negative cathodic overvoltage.

(vi) For the anode potential it follows that $E_{rev,A}$ is equal to $E_{rev,cell}$ [4].

$$E_{rev,A} = E_{rev,cell}; E_{rev,cell} = 1.23\,V\ [2] \tag{31}$$

for the temperature and composition given above. The anode overvoltage was approximated by a Tafel equation

$$\eta_A = a + b\log(j) \tag{32}$$

where j is in A cm^{-2}, and $a = 0.5$ V and $b = 0.25$ V decade^{-1} [2].

From Equations 31, 32 and Equation 3 the definition of $A(i,j,k,l)$ needed for the use of Equations 18–21 follows:

$$A(i,j,k,l) = E_{rev,cell} + a + b\log(j) \tag{33}$$

Equation 33 is valid for the point (i,j) located in the anode and the point near the boundary located outside the anode (i.e., in the electrolyte).

(vii) The condition of symmetry through the centre of the vertical stud in Fig. 1 (in the y-direction) was used. The condition of symmetry was the same as the condition of the insulated wall: no current was flowing in the direction normal to the plane of symmetry.

(viii) The anode contour line was derived by averaging four measured industrial anode shapes [7]. The slope of the averaged anode contour near the electrolyte level (below it) corresponds to the angle $\alpha = 80°$ to the horizontal.

(ix) It was assumed that the side of the anode coming into the electrolyte is vertical. In reality it is subjected to burning in air and has an angle of a few degrees less than 90°.

4. Calculation procedure

(i) For a 2D cross-section of the industrial cell represented in Fig. 1 the Galvani potentials were calculated. The whole space was divided into rectangles 0.4 cm × 0.4 cm. (i.e., $d = 0.2$ cm, see Equation 17).

(ii) For modelling the shape of the anode boundary diagonals of the rectangles were also used. For the equation of currents in that case see the explanation given below. The conservative scheme is valid for elements crossed by a diagonal boundary as well.

(iii) Starting values of the Galvani potentials were estimated on the assumption that the average anode current density is 0.8 A cm^{-2}. These starting values were also used for the calculation of $A(i,j,k,l)$ values around the anode boundary.

(iv) To improve these potentials the successive overrelaxation method (SOR) was used, this being an iterative method. In each iteration the potential in the point (i,j) is improved so as to better fulfil the condition given by Equation 25. The iteration procedure was used as many times as necessary until the desired threshold (accuracy) for all potentials (in all (i,j) points) was reached.

(v) When the threshold was reached (10^{-10} V) for all $\varphi(i,j)$, all values of $A(i,j,k,l)$, (see Equation 33), around the anode boundary, as well as the potentials of the anode boundary, were corrected using the newly calculated current density. Also, the potentials at the cathode boundary were corrected using the newly calculated currents. To minimize instabilities in $A(i,j,k,l)$ only a certain fraction of the newly calculated values of $A(i,j,k,l)$ was used.

(vi) When the selected threshold for ΔA (10^{-6} V) was reached, the calculation was terminated.

(vii) For the approximation of the curvilinear boundary of the anode (see Fig. 1) several techniques were used: two different approximations of a rectangular boundary (lower and upper approximation), and two different approximations of a diagonal boundary (diagonal boundary with and without fluxes along the diagonal boundary). These four cases are illustrated in Fig. 5, where the approximation lines of the anode boundary are shifted sidewise to display the anode boundary more clearly.

For the rectangular approximation of the curvilinear boundary the above mentioned formulae were used while the formulae for the diagonal approximation are given in the following. The scheme of a diagonal approximation of one case is given in Fig. 6, where the case of an element located in the electrolyte near the anode surface is shown. Due to the diagonal approximation, a point which is in the neighbourhood of a boundary does not have the same fluxes as in the rectangular 2D elements. Two fluxes are crossing the diagonal boundary, $I_{4,1}$ and $I_{2,3}$, see Equations 34 and 35.

$$\mathbf{I}_{4,1} = \mathbf{I}_{2,3} \tag{34}$$

$$\mathbf{I}_{4,1} = \frac{\varphi(i+1,j+1) - \varphi(i,j) - A(i,j,4,1)}{\rho(i+1,j+1) + \rho(i,j)} \tag{35}$$

The difference between the diagonal approximation with current flow along the diagonal boundary and the same approximation without currents along the boundary, lies in the fact that in the latter case, the two fluxes along the boundary in both diagonal directions (up and down) are neglected, see Fig. 6. These new fluxes $\mathbf{I}_{4,2}$ and $\mathbf{I}_{2,4}$ (see dotted arrows in Fig. 6) have the following formulae:

$$\mathbf{I}_{4,2} = \frac{\varphi(i-1,j+1) - \varphi(i,j)}{\rho(i-1,j+1) + \rho(i,j)} \tag{36}$$

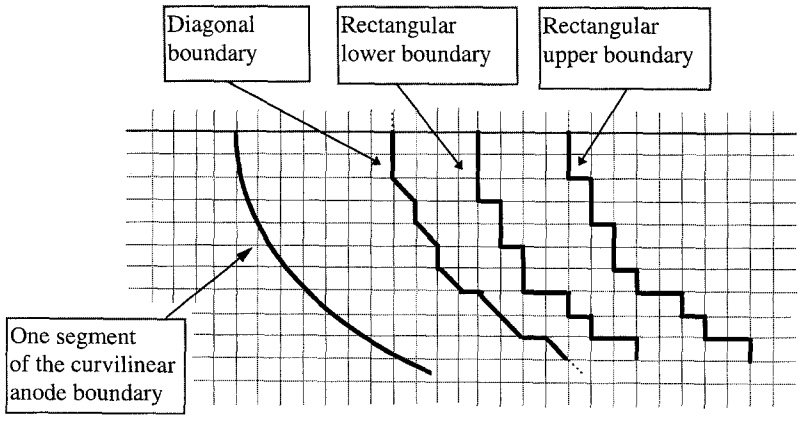

Fig. 5. Curved anode boundary approximation by four different methods: diagonal boundaries, lower rectangular boundary, and upper rectangular boundary.

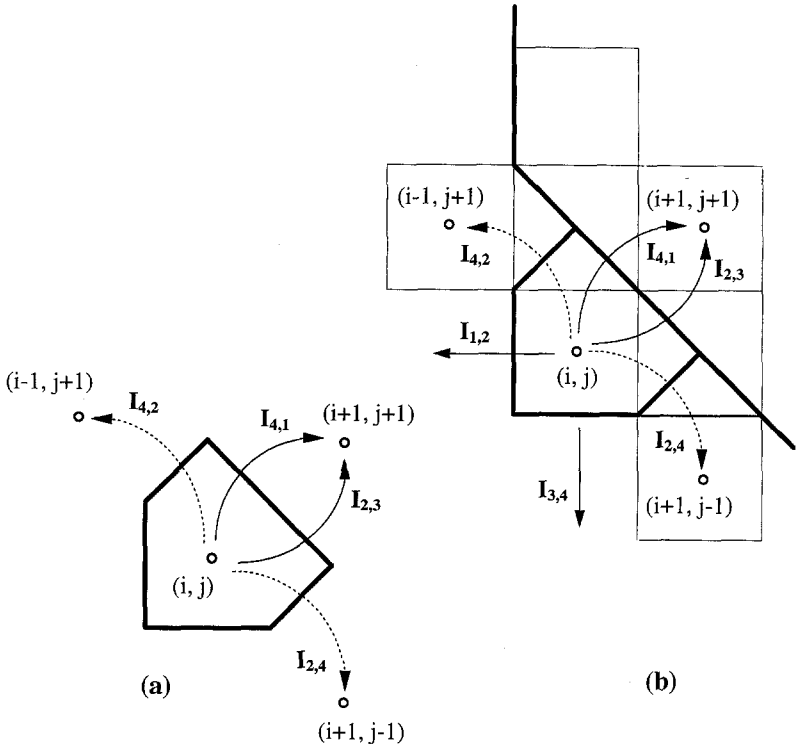

Fig. 6. Curved boundary approximation using diagonal boundary: (a) the shape of the diagonal element, (b) position of the diagonal element

$$\mathbf{I}_{2,4} = \frac{\varphi(i+1,j-1) - \varphi(i,j)}{\rho(i+1,j-1) + \rho(i,j)} \tag{37}$$

The residuum was also modified in accordance with these changes.

5. Results

One of the measured sets of data presented in Part I of this paper, denoted A, was used for comparison. Set A has a slope of the anode contour line near the electrolyte level corresponding to the angle $\alpha = 80°$. The calculated equipotential lines in the electrolyte, shown in Fig. 7, are close to the lines based on the measured data [1]. The deviation of the calculated equipotential lines from the measured data was less than 10%.

The space filled with the electrolyte can be divided into two zones. The first zone has a varying potential gradient (shown by the varying distance between the equipotential lines), which is typical for the area under the near vertical and curved part of the anode. In the second zone, encompassing the horizontal part of the anode, the equipotential lines are equidistant, where the current densities can be regarded as being constant. All the equipotential lines except the uppermost one are located in the electrolyte bulk. The upper equipotential line is placed very close to the anode

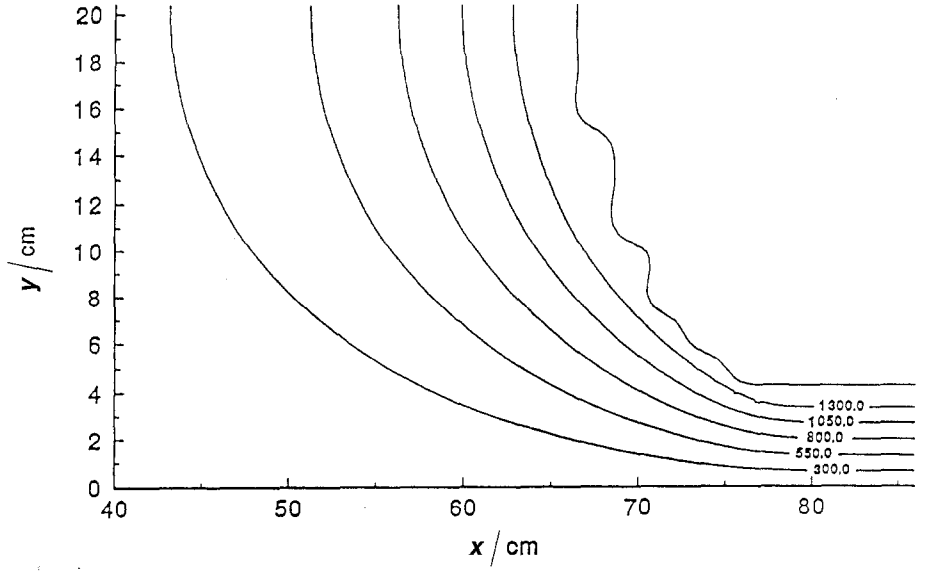

Fig. 7. Calculated equipotential lines in the electrolyte at the side of the Søderberg anode (units in mV). The upper line (without value in mV) is very close to the anode boundary. Origin of the y axis is located at the level of aluminium.

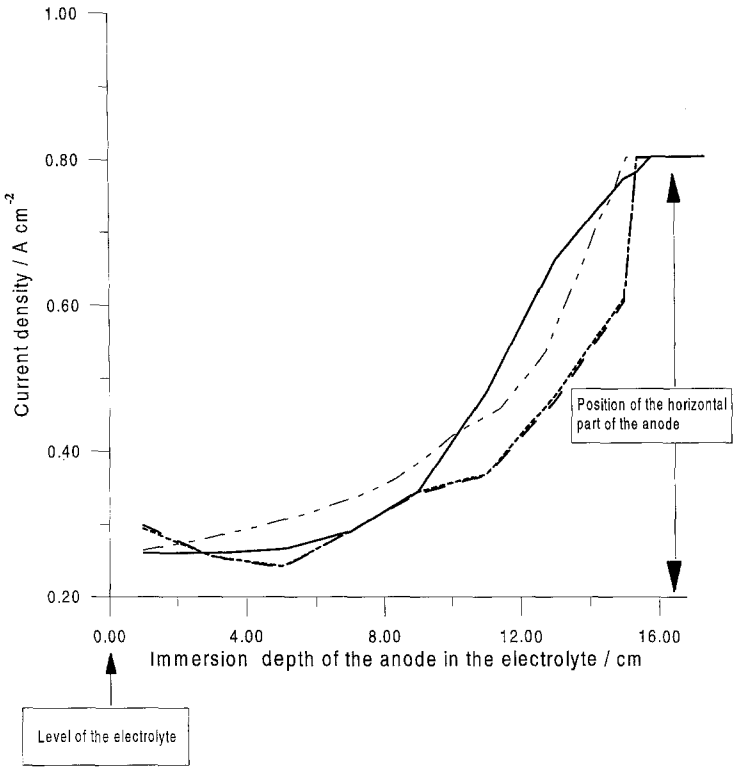

Fig. 8. The current density at the side of the anode as a function of the depth of immersion. Calculation using diagonal boundary approximation. Origin of the y axis is located at the level of the electrolyte. Key: (.....) diagonal boundary; (- - - - -) diagonal boundary with currents along boundary; (————) measured values; (— - - — - - -) FEM.

surface and is obtained using an extrapolation made by the graphics software. The shape of the anode surface contour is not smooth due to the method used for the anode surface approximation, see Fig. 5, that is, a diagonal boundary.

In Figs 8 and 9 the measured [1] and the calculated values of the current density (c.d.) can be compared. The measured values are averaged current densities on the anode surface. For depths more than 10 cm below the surface, measured from the upper level of the electrolyte, the measured data were uncertain because of problems in positioning the probe. The present calculation gave local current densities for all (i,j) points. These values were averaged before plotting in Figs 8 and 9.

For the conservative scheme the local current densities (from the calculation) were averaged over the projection line going from the upper left corner to the lower right corner of the averaging interval; so-called averaging over a diagonal line, as shown in Fig. 10.

The calculated results, based on the conservative scheme were averaged over diagonal lines covering the

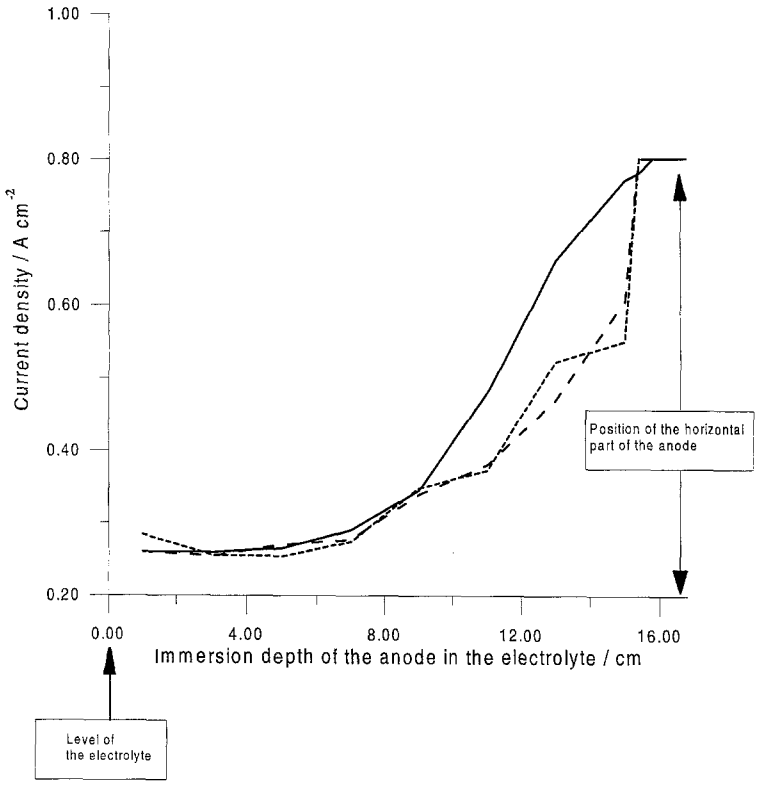

Fig. 9. The current density at the side of the anode as a function of the depth of immersion. Calculation using rectangular boundary approximation. Origin of the y axis is located at the level of the electrolyte. Key: (.....) upper rectangular boundary; (- - - - -) lower rectangular boundary; (————) measured values.

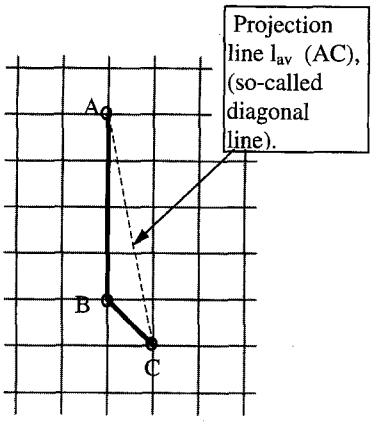

Fig. 10. The scheme of averaging current densities (averaging over the projection line l_{av} going from the upper left hand corner to the lower right hand corner, the so-called diagonal line), see equation 42.

relative height of five calculation units (2 cm). Both the local current densities calculated by the conservative scheme, and the measured local current densities at the side of the anode, close to the surface of the electrolyte, were in the range 0.26–0.28 A cm^{-2}. For the lower part of the anode side the calculated current densities were lower than the measured values. This could firstly be due to the fact that bubble effects were not considered, or secondly that the mesh distance (d) was not small enough, that is, the anode contour was not approximated by a smooth curve, due to the mathematical method used. To check the influence of the curvilinear boundary approximation on the calculation, the finite element method (FEM) [4, 8] was used. With the finite element method the anode contour was approximated by a smoother curve and the local c.d.'s are closer to the measured values in that zone, as shown in Fig. 9. For the conservative scheme it can be seen that calculated and measured values are close on the side near the anode (the differences are 10–15%). On the curved part of the anode boundary the calculated values are lower than the measured values (the differences are 20–28%). In this area there were problems with the access of the probe (see [I]) so the measured curves were uncertain.

The local c.d.'s obtained by FEM are higher than those obtained by the conservative scheme. On the vertical part of the anode the calculated values by FEM are about 15% higher than the measured values. On the curved part of the anode the values of the local c.d. obtained by FEM are closer to the measured values than those obtained by the conservative scheme. In Fig. 9 the calculated current density using rectangular boundaries with averaging over diagonal lines are shown. It can be observed that generally the averaging effects are similar, but on the side of the anode the differences between calculated and measured values are lower for the lower rectangular approximation than for the upper. The averaging over diagonal lines, which is very close to the averaging done during the measurement of equipotential lines, minimizes the influences of the boundary approximation on the local current densities. On the horizontal part of the anode the difference is only about 3%. In Fig. 11 the local c.d.'s along the

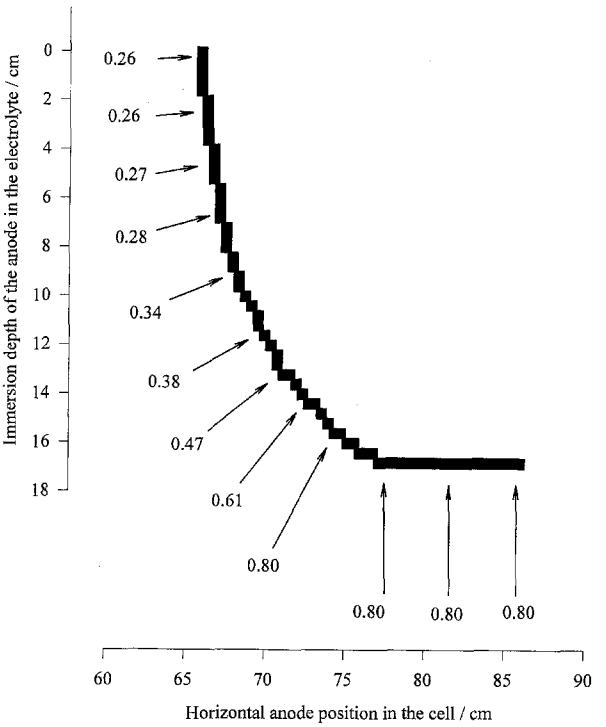

Fig. 11. Current densities (in A cm^{-2}) along anode boundary calculated using diagonal boundary approximation. Values of c.d.'s with their horizontal and vertical position. Origin of the y axis is located at the level of the electrolyte.

anode boundary are shown. The position and values of local c.d. can be seen together with its positions in the x and y directions.

Two methods were used in this study for solution of the Laplace equation: the conservative scheme and the FEM. The advantage of the conservative scheme issues from the fact that summing the currents on the anodic and cathodic side leads to the total current values with an error comparable to that of the potential. In this way the correct implementation of the conservative scheme may be simply checked. The use of the conservative scheme for the complex cell geometry requires complex software. The FEM uses one equation for all triangles, filling 2D space of any geometry. On the software market good mesh generators for the FEM are available. It was necessary to develop, for the studied case, the FEM solver for the secondary current distribution.

References

[1] Z. Kuang and J. Thonstad, *Light Metals* (1994), 667–75.
[2] K. Grjotheim, C. Krohn, M. Malinovsky, K. Matiasovsky and J. Thonstad, 'Aluminium Electrolysis', 2nd edn, Aluminium-Verlag, Dusseldorf (1982).
[3] K. Grjotheim and H. Kvande, 'Introduction to Aluminium Electrolysis', Aluminium-Verlag, Dusseldorf (1993).
[4] I. Rousar, K. Micka and A. Kimla, 'Electrochemical Engineering', Academia, Praha and Elsevier, Amsterdam (1986) pp. 123–7.
[5] B. Steffen and I. Rousar, *Electrochim. Acta* **40** (1995) 379.
[6] J. Hives, J. Thonstad, A. Sterten and P. Fellner, *Light Metals* (1994) 187.
[7] Z. Kuang, PhD thesis, The Norwegian Institute of Technology, Trondheim, 1994.
[8] O. C. Zienkiewicz, 'The Finite Element Method in Engineering Science', McGraw-Hill, London (1971).